Responsive Batteries

Deutsche Ausgabe: DOI: 10.1002/ange.201608163
Internationale Ausgabe: DOI: 10.1002/anie.201608163

A Responsive Battery with Controlled Energy Release

*Xiaopeng Wang, Jian Gao, Zhihua Cheng, Nan Chen, and Liangti Qu**

Abstract: *A new type of responsive battery with the fascinating feature of pressure perceptibility has been developed, which can spontaneously, timely and reliably control the power outputs (e.g., current and voltage) in response to pressure changes. The device design is based on the structure of the Zn–air battery, in which graphene-coated sponge serves as pressure-sensitive air cathode that endows the whole system with the capability of self-controlled energy release. The responsive batteries exhibit superior battery performance with high open-circuit voltage (1.3 V), and competitive areal capacity of 1.25 mAh cm^{-2}. This work presents an important move towards next-generation intelligent energy storage devices with energy management function.*

With increasing popularization of portable electronics and electric vehicles worldwide, electrochemical energy storage devices such as batteries and supercapacitors are becoming critically important in our daily life. However, for future energy storage devices, it would be terrific if their deformable, wearable, implantable and even responsive and perceptual characteristics could be combined with advanced electronic devices. In this regard, advance has been made in recent years to develop novel energy supply systems including compressible or stretchable supercapacitors and batteries,[1–5] fabric photovoltaics,[6] and implantable miniature batteries.[7]

Smart stimulus-responsive systems that can spontaneously respond to external variation such as magnetic field, force, light, moisture, and other stimuli,[8–13] have been attracting considerable attention due to their promising applications in biomedicine,[14,15] active identifications,[16] and nanosensor[17] field. In particular, graphene is identified as a beneficial additive or an effective responsive component by itself to improve the conductivity, flexibility, mechanical strength and/or the overall responsivity performance of smart devices.[18] As demonstrated by us and other groups, advanced graphene-based responsive systems including fibre robots and motors,[19,20] human breathing monitors,[21] drug delivery[22] and smart skins[23] have been developed which are capable of responding to moisture, temperature, and force variation. However, for the current energy storage devices, the capability to apperceive and respond to environmental changes in a spontaneous, timely and reliable manner is generally absent.

[*] X. P. Wang, J. Gao, Z. H. Cheng, Dr. N. Chen, Prof. L. T. Qu
Beijing Key Laboratory of Photoelectronic/Electrophotonic Conversion Materials, Key Laboratory of Cluster Science, Ministry of Education of China, School of Chemistry and Chemical Engineering, Beijing Institute of Technology
Beijing 100081 (P.R. China)
E-mail: lqu@bit.edu.cn

Supporting information for this article can be found under: http://dx.doi.org/10.1002/anie.201608163.

Herein, we develop a new type of energy management device with the fascinating feature of environmental pressure perceptibility. A tactile sensing battery has been designed on the basis of the pressure-sensitive graphene-coating sponge electrodes, which can spontaneously and accurately control the power outputs (e.g., current and voltage) of the whole battery upon different pressure stimulations. In addition, this newly developed batteries exhibit outstanding battery performances such as a high open-circuit voltage of 1.3 V, areal capacities of 1.25 mAh cm^{-2}, and a high energy density of 1200 Wh L^{-1}. More interestingly, rechargeable tactile sensing batteries were integrated in series to power the commercial light-emitting diodes exemplifying the feasibility for practical applications as compressible power sources and energy management devices in optoelectronics. This responsive battery demonstrated here will advance the development of smart energy devices with the capability of user-device interactions.

To achieve the tactile sensing battery, we first fabricated a pressure-sensitive sponge electrode (PSE) by coating the conductive graphene sheets on the backbones of commercial polyurethane sponge through dip-coating. The as-fabricated PSE functions as both the output power-controller and cathode in the final battery. The overall fabrication procedure of PSE is shown in Figure 1a. A graphene oxide (GO) aqueous solution with a certain concentration was adsorbed into the polyurethane sponge, allowing the assembly of GO sheets along the framework. After drying and thermal annealing (see Supporting Information (SI) for details) a conductive coating layer of reduced graphene oxide (RGO) was formed on the sponge backbone, followed by a color change from the yellow to black. X-ray diffraction (XRD) and Raman measurements provided evidence for GO reduction (Figures S1 and S2 in the SI). The polyurethane sponge framework becomes rough and crinkled after coating with graphene sheets (Figure 1b and c), indicating the effective attachment of graphene sheets on the framework to form the conductive network. PSEs can be compressed by more than 90% (Figure 1d), and the unloading curves almost return to the initial points, suggesting complete shape recovery without mechanical failure. Compressive stress of 150 kPa for PSEs indicates their great potential for applications in compressible electrodes. The compressive strain (ε) dependence of the electrical resistance (R) is given in Figure 1e. The normalized electrical resistance (R/R_0) decreases conformably with an increase of ε under the measured region of up to 90%, displaying a strong ε dependence on electric resistance.

When the PSE is employed as the cathode and current collector in the newly developed tactile sensing battery (TSB), it is not only to endow the whole device with compressibility, but also serves as the power controller in

 © 2016 Wiley-VCH Verlag GmbH & Co. KGaA, Weinheim

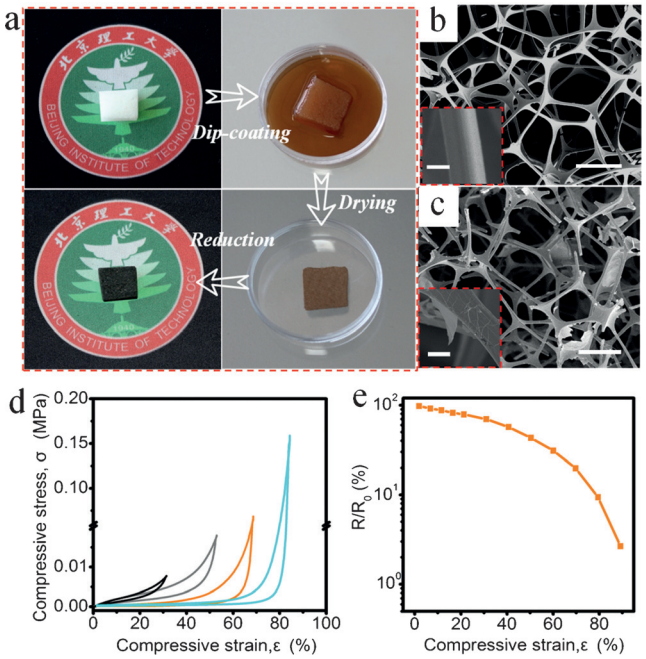

Figure 1. a) Fabrication procedure of PSEs through a three-step strategy, including dip-coating, drying and reduction. b, c) Scanning electron microscopy (SEM) images of the commercial polyurethane sponge and graphene-coated PSEs. Insets are the corresponding magnified SEM images of the sponge frameworks. d) Stress–strain curves of PSE with different strains of 30%, 50%, 70% and 90%, respectively. e) Electrical resistance variation of the PSEs as a function of compressive strain ε. Scale bars: (b) and (c) 100 μm, insets of (b) and (c) 2 μm.

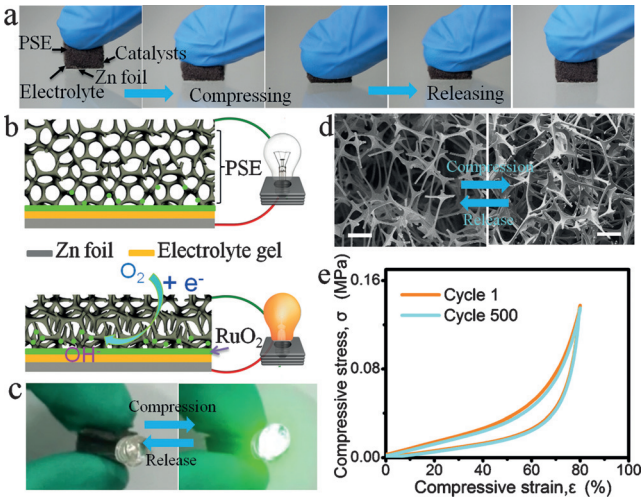

Figure 2. a) Optical photograph showing the structure of TSB, and the compression–recovery process displaying that TSBs recover their original shape after compression of ca. 80%. b) Schematic structure and working principle of TSB under compression. c) Loading of a compressive force onto a TSB increases its output power, lighting the green LED. d) SEM images of PSE network under mechanical deformation. e) Cyclic stress–strain curves of TSBs at 80% strain at the pressure of 140 kPa. Scale bar: d) 100 μm.

the TSB. The fabricated TSB can be compressed and completely recovers to the original state (Figure 2a). The configuration of the TSB is essentially based on the sandwich model, where a KOH-based electrolyte hydrogel was sandwiched between PSE cathode and Zn foil anode (10 μm thick). RuO_2 nanoparticles were attached to the surface of the electrolyte gel and PSE and catalyzed the oxygen evolution reaction (OER) in the charging process (see the SI for details). All components are inspired from the typical structure of the Zn–air battery which is characterized by a relatively high capacity making it suitable for long-term power supply in next-generation electronics.

To understand the mechanism of pressure-controlled power output of TSB, we need to straighten two points on the discharging procedure of Zn–air batteries as follow: 1) During discharge, oxygen is reduced at the air cathode surface and attracts electrons from the electrolyte; this process can take place in the absence of catalysts. 2) Generally, RGO could dictate the number of the electrochemically active sites available for oxygen reduction reaction (ORR) by adsorbing oxygen from the atmosphere.[24] This means that increasing the electrolyte–PSE interface with more reaction sites in RGO is beneficial for obtaining higher output current and voltage. Thus, we assumed that the controllability of the output power of TSB is related to the variation of the contact area of the interface between the electrolyte gel and PSE resulting in a change of electronic carrier concentration upon changing pressure loading, which is schematically shown in Figure 2b. With increasing pressure on TSB, the PSE increases contact with the electrolyte gel, thus creating a larger contact area of the interface. Meanwhile, the RGO within PSE absorbs oxygen from the atmosphere and provides reaction sites for the reduction of O_2 to OH^- in the alkaline electrolyte gel, resulting in an increased electronic carrier concentration on the surface of the electrodes and an enhanced output power. Vice versa, TSB converts to low power output mode in response to a decrease in pressure loading. Moreover, the impedance spectra (Figure S3) of TSB at different compression strains also demonstrated that the transport of charge carriers was improved upon increasing pressure loading. Thus, the power output of TSB can be controlled by compression.

Figure 2c displays the change of output power in response to external pressure through a green light-emitting diode (LED) integrated in TSBs (Movie S1 in the SI). During the compression process, the compressive deformation of the graphene-coated polyurethane network within PSE can be clearly observed in Figure 2d. The excellent mechanical robustness of TSB was further demonstrated through a negligible plastic deformation after 500 cycles at a maximum external pressure of 140 kPa at $\varepsilon = 80\%$ (Figure 2e). The mechanical properties of TSBs are also shown in Figure S4, further demonstrating their potential application in compressible batteries.

The battery performance was evaluated to demonstrate the feasibility of TSBs to be operated under ambient conditions. All the following electrochemical tests are based on the completely compressed state of TSB at $\varepsilon = 80\%$. Galvanostatic discharge measurements were conducted at a current density of 0.1 mA cm^{-2} as shown in Figure 3a. It can

© 2016 Wiley-VCH Verlag GmbH & Co. KGaA, Weinheim

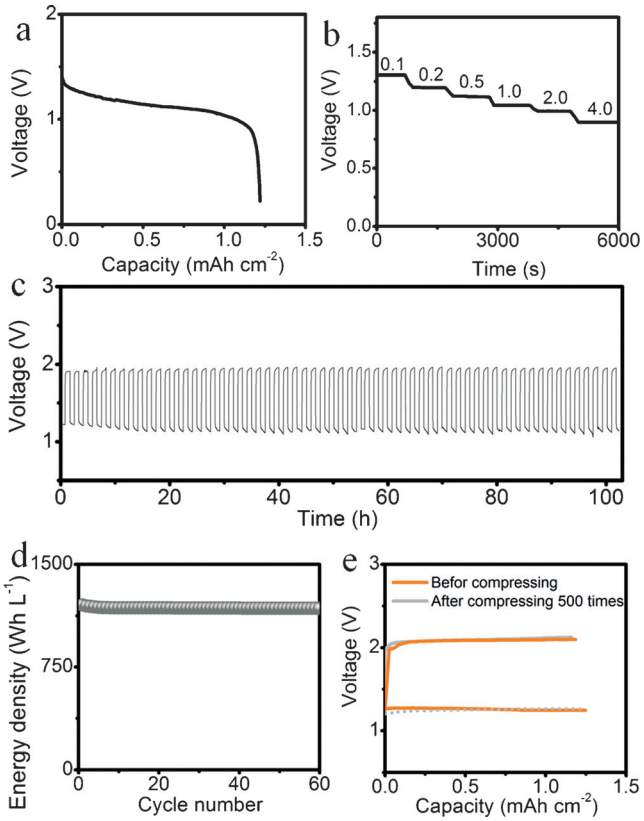

Figure 3. a) Galvanostatic discharge curves of the TSB at current density of 0.1 mA cm^{-2}. b) Rate discharge curves of TSB at different current densities (0.1, 0.2, 0.5, 1, 2 and 4 mA cm^{-2}, respectively). c) Galvanostatic discharge–charge cycling curves of the all-solid-state TSB at a current density of 0.1 mA cm^{-2}. d) Energy densities of the zinc–air battery using PSE as air cathode. e) Discharge–charge voltage plateaus of TSB before and after compressing for 500 times.

be seen that more than 90% of the capacity can be stably released with a relatively constant voltage platform during discharge process, and an outstanding discharge capacity of ca. 1.25 mAh cm^{-2} is achieved. The discharge voltage plateaus decreased with increasing current densities (Figure 3b). The TSB with PSE cathode showed voltage plateaus of ca. 1.3 V at 0.1 mA cm^{-2} discharge rate. The value is higher than other recently report values.[25] The remarkable discharging properties could be attributed to the limited gas diffusion within the compressible PSE microstructure.[26] After attachment of the RuO_2 nanoparticles (OER catalyst) on the surface of the electrolyte gel and PSE through impregnation, the TSB is rechargeable. An energy-dispersive X-ray spectrometry (EDXS) map (Figure S5) reveals the existence and homogeneous distribution of the RuO_2 nanoparticles coated on the surface of the electrolyte gel. Meanwhile, RGO within PSE serves as support for nano-sized RuO_2 (Figure S6), and thus the PSE cathodes are responsible for the synergistic OER activity during the charging procedure (Figure S7).

Our Zn–air battery based on PSE air cathode exhibited high reversibility and afforded discharge–charge cycles at a current density of 0.1 mA cm^{-2} without obvious voltage change over 60 cycles for 100 h (Figure 3c and Figure S8). It outperforms most of the recently reported Zn–air batteries (see Table S1 in the SI). Furthermore, the energy efficiency of TSB is about 66% at the initial stage and maintained at 61% over 100 h (Figure S9), demonstrating a remarkable catalytic stability of the air cathode. In Figure 3d, the calculated energy density of our Zn–air battery was 1200 Wh L^{-1} (based on the zinc film volume), which is much higher than for common lithium-ion batteries (about 220 Wh L^{-1}).[27] In Figure 3e, we evaluated the charge–discharge performances of our battery before and after compressing for 500 cycles. The results demonstrate that the electrochemical capacity and charge–discharge voltage remained almost unchanged, indicating the electrochemical performance of TSB was almost unaffected after repeated compressing. The self-discharge rate of TSB was 5% per month by calculating the capacity fade during storage in a glove box (filled with argon) for 100 h (Figure S10).

To investigate the controllable output power behavior, the voltage and current outputs of TSB were measured as a function of compressive strain in a strain deformation range of $0 < \varepsilon < 80\%$. As shown in Figure 4a, the output voltages monotonically increase with the applied pressure of up to 140 kPa at $\varepsilon = 80\%$. The maximum output voltage of

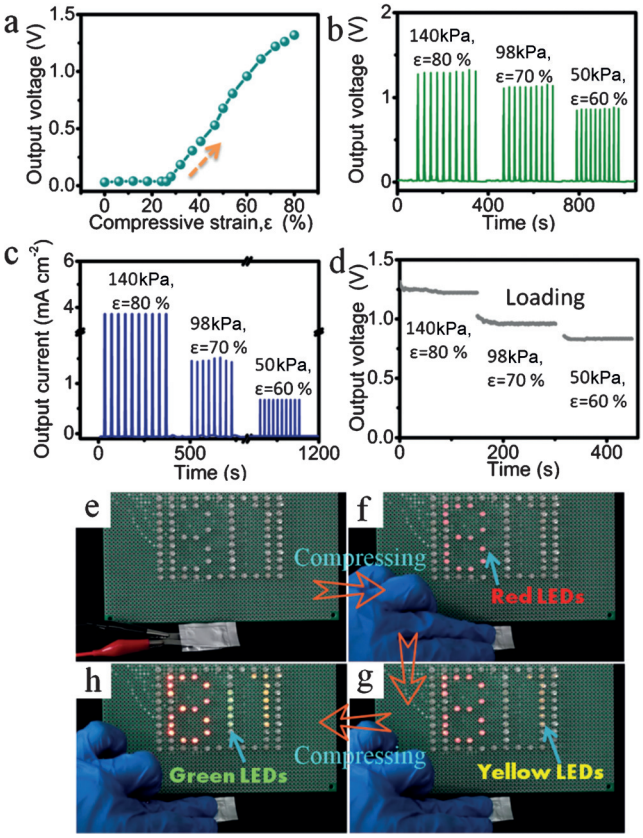

Figure 4. a) Output voltage of the TSBs under continually compressive strains at a speed of 0.2 mm s^{-1}. b, c) Self-regulated output voltage (b) and current (c) performances of TSBs under various compressive strains. d) Continuous output voltage performances under different pressure loading. e–h) Two in-serial connected TSBs were semi-packaged to light LEDs in the order of red LEDs (marked "B"), yellow LEDs (marked "T") and green LEDs (marked "I") with increase of applied pressure.

© 2016 Wiley-VCH Verlag GmbH & Co. KGaA, Weinheim

1.31 V is obtained when the effective contact area of PSE network reaches saturation at maximum strain deformation. Real-time monitoring of the output voltage of TSB during compression is shown in Movie S2 in the SI. The dependence of voltage output on external pressure is also shown in Figure 4b. The output voltages of TSB increased progressively with increasing pressure, and were maintained at a constant pressure level, indicating the reliable power release during external pressure stimuli. Accordingly, current outputs show similar regularity in response to external pressure (Figure 4c). This capability makes the TSB unique among other traditional electrochemical batteries. For example, the responsive battery can output pulse voltage and current with regular magnitude. Based on the maximum pulse power outputs of ca. 5 mW cm^{-2}, it is able to power around 720 times of continuous pressure pulses with 1 s interval time on a single charge. Moreover, it is worth noting that the TSB can also provide continuous voltage outputs at a continuous pressure applied, which is critical for practical applications. As shown in Figure 4d, the continuous voltage outputs of TSB increased with increasing applied pressure during galvanostatic discharge (0.1 mA cm^{-2}). Thus, TSB is capable of reliably controlling the power output by the tunable external pressure-stimuli without need of conventional battery management system. The newly developed controlled energy release of TSB is visually demonstrated in Figure 4e–h and Movie S3 in the SI. In this way, different LED colors were turned on in a specified order, which are operated at different voltage ranges of 1.8–2.1 V (red LEDs), 1.9–2.2 V (yellow LEDs) and 2–2.2 V (green LEDs). Semi-packaged TSBs were integrated to initially power the red LEDs (Figure 4f), followed by the yellow LEDs (Figure 4g), and then green LEDs (Figure 4h) with increasing the applied pressure, indicating that the power output of TSB increased gradually during the whole compression process.

The dynamic responsiveness of TSB was further measured by a linear electrodynamic shaker, which was repeatedly pressed for different times in per unit time of 50 s. Figure 5 shows the response waveforms of the TSB subjected to compressions at 4, 8, 16 and 32 times per unit of 50 s. All acquired signals in the dynamic tactile tests are based on the maximum pressure loading (140 kPa) of TSB device. The measured output voltages and output currents of TSB are stable and uniform at arbitrary test cycles, without detectable variation across all the dynamic tests as shown in Figure 5a and b. As can be seen, the TSB is able to provide a reliable working state in response to dynamic force. In addition, TSB responds fast and synchronous to pressure (Figure 5c,d). The output voltage and current signal show an instantaneous response with the applied pressure. The delay, which is defined as the maximum delay time of output signal to input pressure divided by the time per cycle of loading and unloading, is quite small for voltage and current signals. From all the above-mentioned results it can be concluded that the pressure-actuated output power control of TSB serves as a reliable management mode for effective energy release.

In summary, we have developed a smart graphene-based tactile sensing battery which displays self-regulatory output power in response to a tactile stimulus. The compressible TSB

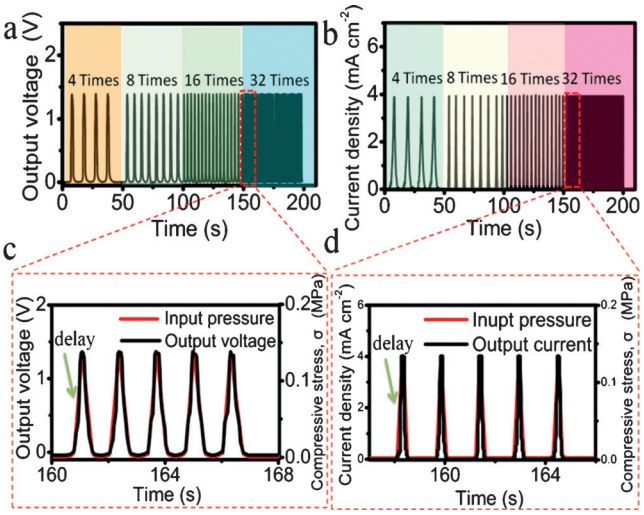

Figure 5. a,b) Measured output voltage (a) and current (b) based on the input pressure at 4, 8, 16 and 32 times per unit of 50 s. c, d) Dynamic response of output voltage (c) and current (d) under a periodically input pressure as a function of time.

is produced from a graphene-coated PSE cathode, a hydrogel polymer electrolyte and a Zn foil anode. Graphene-coated PSE serves both as power controller and air cathode in the TSB. Based on the pressure sensitivity of PSE, the output power of TSB can readily and reliably controlled by applied pressure. The self-regulated output power of TSBs has been visually demonstrated in the proof-of-concept LED lighting test. Furthermore, as energy storage device, the TSB exhibits outstanding areal capacities (1.25 mAh cm^{-2}), stable discharge voltage plateaus of 1.3 V, and an outstanding energy density (1200 Wh L^{-1}). We believe the current study of perceptual energy storage devices with self-regulation power management stands for an important advance in the field of power sources for smart technologies.

Acknowledgements

This work was supported by the NSFC (No. 21325415, 21301018, 51673026), the National Basic Research Program of China (2011CB013000), and the Beijing Natural Science Foundation (2152028).

Keywords: energy management · graphene sponge · pressure-responsive battery · zinc–air battery

How to cite: *Angew. Chem. Int. Ed.* **2016**, *55*, 14643–14647
Angew. Chem. **2016**, *128*, 14863–14867

[1] Z. Niu, H. Dong, B. Zhu, J. Li, H. H. Hng, W. Zhou, X. Chen, S. Xie, *Adv. Mater.* **2013**, *25*, 1058–1064.
[2] C. Xu, Z. Li, C. Yang, P. Zou, B. Xie, Z. Lin, Z. Zhang, B. Li, F. Kang, C. P. Wong, *Adv. Mater.* **2016**, *28*, 4105–4110.
[3] Y. Zhao, J. Liu, Y. Hu, H. Cheng, C. Hu, C. Jiang, L. Jiang, A. Cao, L. Qu, *Adv. Mater.* **2013**, *25*, 591–595.
[4] W. Liu, Z. Chen, G. Zhou, Y. Sun, H. R. Lee, C. Liu, H. Yao, Z. Bao, Y. Cui, *Adv. Mater.* **2016**, *28*, 3578–3583.

© 2016 Wiley-VCH Verlag GmbH & Co. KGaA, Weinheim

[5] L. Hu, M. Pasta, F. L. Mantia, L. Cui, S. Jeong, H. D. Deshazer, J. W. Choi, S. M. Han, Y. Cui, *Nano Lett.* **2010**, *10*, 708 – 714.
[6] Z. Yang, H. Sun, T. Chen, L. Qiu, Y. Luo, H. Peng, *Angew. Chem. Int. Ed.* **2013**, *52*, 7545 – 7548; *Angew. Chem.* **2013**, *125*, 7693 – 7696.
[7] F. Albano, M. Chung, D. Blaauw, D. Sylvester, K. Wise, A. Sastry, *J. Power Sources* **2007**, *170*, 216 – 224.
[8] G. Zabow, S. Dodd, A. Koretsky, *Nature* **2015**, *520*, 73 – 77.
[9] Y. Fang, Y. Ni, S.-Y. Leo, C. Taylor, V. Basile, P. Jiang, *Nat. Commun.* **2015**, *6*, 7416 – 7423.
[10] L. Qiu, M. Bulut Coskun, Y. Tang, J. Z. Liu, T. Alan, J. Ding, V. T. Truong, D. Li, *Adv. Mater.* **2016**, *28*, 194 – 200.
[11] H. B. Yao, J. Ge, C. F. Wang, X. Wang, W. Hu, Z. J. Zheng, Y. Ni, S. H. Yu, *Adv. Mater.* **2013**, *25*, 6692 – 6698.
[12] Y. Tai, G. Lubineau, Z. Yang, *Adv. Mater.* **2016**, *28*, 4665 – 4670.
[13] X. Chen, D. Goodnight, Z. Gao, A. H. Cavusoglu, N. Sabharwal, M. DeLay, A. Driks, O. Sahin, *Nat. Commun.* **2015**, *6*, 7346 – 7452.
[14] C. Dagdeviren, Y. Shi, P. Joe, R. Ghaffari, G. Balooch, K. Usgaonkar, O. Gur, P. L. Tran, J. R. Crosby, M. Meyer, *Nat. Mater.* **2015**, *14*, 728 – 736.
[15] H. Lee, T. K. Choi, Y. B. Lee, H. R. Cho, R. Ghaffari, L. Wang, H. J. Choi, T. D. Chung, N. Lu, T. Hyeon, *Nat. Nanotechnol.* **2016**, *11*, 566 – 572.
[16] K. Hu, R. Xiong, H. Guo, R. Ma, S. Zhang, Z. L. Wang, V. V. Tsukruk, *Adv. Mater.* **2016**, *28*, 3549 – 3556.
[17] B. Zhu, H. Wang, Y. Liu, D. Qi, Z. Liu, H. Wang, J. Yu, M. Sherburne, Z. Wang, X. Chen, *Adv. Mater.* **2016**, *28*, 1559 – 1566.
[18] J. Zhang, L. Song, Z. Zhang, N. Chen, L. Qu, *Small* **2014**, *10*, 2151 – 2164.
[19] H. Cheng, J. Liu, Y. Zhao, C. Hu, Z. Zhang, N. Chen, L. Jiang, L. Qu, *Angew. Chem. Int. Ed.* **2013**, *52*, 10482 – 10486; *Angew. Chem.* **2013**, *125*, 10676 – 10680.
[20] H. Cheng, Y. Hu, F. Zhao, Z. Dong, Y. Wang, N. Chen, Z. Zhang, L. Qu, *Adv. Mater.* **2014**, *26*, 2909 – 2913.
[21] F. Zhao, Y. Zhao, H. Cheng, L. Qu, *Angew. Chem. Int. Ed.* **2015**, *54*, 14951 – 14955; *Angew. Chem.* **2015**, *127*, 15164 – 15168.
[22] Y. Pan, H. Bao, N. G. Sahoo, T. Wu, L. Li, *Adv. Funct. Mater.* **2011**, *21*, 2754 – 2763.
[23] H. H. Chou, A. Nguyen, A. Chortos, J. W. To, C. Lu, J. Mei, T. Kurosawa, W. G. Bae, J. B. H. Tok, Z. Bao, *Nat. Commun.* **2015**, *6*, 8011 – 8020.
[24] Y. Liang, Y. Li, H. Wang, J. Zhou, J. Wang, Tom Regier, H. Dai, *Nat. Mater.* **2011**, *10*, 780 – 786.
[25] Y. Xu, Y. Zhang, Z. Guo, J. Ren, Y. Wang, H. Peng, *Angew. Chem. Int. Ed.* **2015**, *54*, 15390 – 15394; *Angew. Chem.* **2015**, *127*, 15610 – 15614.
[26] S. Sandhu, J. Fellner, G. Brutchen, *J. Power Sources* **2007**, *164*, 365 – 371.
[27] Y. Nishi, *J. Power Sources* **2001**, *100*, 101 – 106.

Received: August 21, 2016
Published online: October 20, 2016

 © 2016 Wiley-VCH Verlag GmbH & Co. KGaA, Weinheim